

Partial Separability and Functional Graphical Models for Multivariate Gaussian Processes

Javier Zapata^{*1}, Sang-Yun Oh², and Alexander Petersen³

^{1,2,3}Department of Statistics and Applied Probability
University of California Santa Barbara
²Lawrence Berkeley Lab, Berkeley, CA

March 26, 2022

Abstract

The covariance structure of multivariate functional data can be highly complex, especially if the multivariate dimension is large, making extension of statistical methods for standard multivariate data to the functional data setting quite challenging. For example, Gaussian graphical models have recently been extended to the setting of multivariate functional data by applying multivariate methods to the coefficients of truncated basis expansions. However, a key difficulty compared to multivariate data is that the covariance operator is compact, and thus not invertible. The methodology in this paper addresses the general problem of covariance modeling for multivariate functional data, and functional Gaussian graphical models in particular. As a first step, a new notion of separability for multivariate functional data is proposed, termed partial separability, leading to a novel Karhunen-Loève-type expansion for such data. Next, the partial separability structure is shown to be particularly useful in order to provide a well-defined Gaussian graphical model that can be identified with a sequence of finite-dimensional graphical models, each of fixed dimension. This motivates a simple and efficient estimation procedure through application of the joint graphical lasso. Empirical performance of the method for graphical model estimation is assessed through simulation and analysis of functional brain connectivity during a motor task.

Keywords: Functional Data; Inverse Covariance; Functional Brain Connectivity

^{*}Corresponding Author

1 Introduction

The analysis of functional data continues to be an important field for statistical development given the abundance of data collected over time via sensors or other tracking equipment. Frequently, such time-dependent signals are vector-valued, resulting in multivariate functional data. Prominent examples include longitudinal behavioral tracking [5], blood protein levels [9], traffic measurements [6, 7], and neuroimaging data [19, 13], for which dimensionality reduction and regression have been the primary methods investigated. As for standard multivariate data, the nature of dependencies between component functions of multivariate functional data constitute an important question requiring careful consideration.

As our motivating data example, we will consider dependencies between fMRI signals for a large number of regions across the brain during a motor task experiment. Since fMRI signals are collected simultaneously, it is natural to consider a multivariate process $\{X(t) \in \mathbb{R}^p : t \in \mathcal{T}\}$, where \mathcal{T} is an interval in \mathbb{R} over which the scans are taken, as a model for the fMRI signals [21]. The dual multivariate and functional aspects of the data make the covariance structure of X quite complex, particularly if the multivariate dimension p is large. This leads to difficulties in extending highly useful multivariate analysis techniques, such as graphical models, to multivariate functional data without further structural assumptions. For example, in the analogous setting of spatio-temporal data, it is common to impose further structure to the covariance, usually assuming that the spatial and temporal effects can be separated in some way. However, similar notions for multivariate functional data have not yet been considered.

As for ordinary multivariate data, the conditional independence properties of X are perhaps of greater interest than marginal covariance, leading to the consideration of inverse covariance operators and graphical models for functional data. If X is Gaussian, each component function X_j is represented by a node in the functional Gaussian graphical model

(FGGM), consisting of a single network of p nodes. This is inherently different from methods seeking to estimate time-dependent graphical models (e.g. [28, 15, 22, 20]). For such models, the graph is dynamic and has nodes corresponding to scalar random variables. In an FGGM, the graph is static while each node represents an infinite-dimensional functional object. This is an important distinction, as covariance operators for functional data are compact and thus not invertible in the usual sense, so that presence or absence of edges cannot in general be identified immediately with zeros in any precision operator. In the past few years, there has been some investigation into FGGMs. [29] developed a Bayesian framework for graphical models on product function spaces, including the extension of Markov laws and appropriate prior distributions. [21] implemented a truncation approach, whereby each function is represented by the coefficients of a truncated basis expansion using functional principal components analysis, and a finite-dimensional graphical model is estimated by a modified graphical lasso criterion. [16] developed a non-Gaussian variant, where conditional independence was replaced by a notion of so-called additive conditional independence.

The methodology proposed in this paper is within the setting of multivariate Gaussian processes as in [21], and we explore notions of separability for multivariate functional data and their implications on the existence and estimation of suitable inverse covariance objects. There are at least three novel contributions of this methodology to the fields of functional data analysis and Gaussian graphical models. First, we define partial separability for multivariate functional data that yields a novel representation termed the partial separability Karhunen-Loève expansion (PSKL), given its similarity to the well-known analog for univariate functional data. The second contribution is to show that, when the process is indeed partially separable, an FGGM is well-defined and can be identified with a sequence of finite-dimensional graphical models. In particular, the FGGM under partial separability overcomes the problem of noninvertibility of the covariance operator when X

is infinite-dimensional, in contrast with [29, 21] which assumed that the functional data were concentrated on finite-dimensional subspaces. Third, we develop an intuitive estimation procedure for the partially separable functional Gaussian graphical model (psFGGM) based on simultaneous estimation of multiple graphical models. Furthermore, theoretical properties are derived under the regime of fully observed functional data. Empirical performance of the psFGGM is then compared to the FGGM method of [21] through simulations involving dense and noisily observed functional data, including a setting where partial separability is not satisfied. Finally, the method is applied to the study of functional brain connectivity using data from the Human Connectome Project (HCP) corresponding to a motor task experiment. Through these practical examples, psFGGM is shown to provide improved efficiency in estimation and computation. We also note that a downloadable version of both PSKL and psFGGM methods has been developed in R, and is freely available at <https://github.com/javzapata/fgm>.

2 Preliminaries

2.1 Multivariate Functional Data

Let $L^2[0, 1]$ denote the space of square-integrable measurable functions on $[0, 1]$ endowed with the standard inner product

$$\langle f, g \rangle = \int_0^1 f(t)g(t) dt$$

and associated norm $\|\cdot\|$. $(L^2[0, 1])^p$ is its p -fold Cartesian product for fixed $p \in \mathbb{N}$, endowed with inner product $\langle f, g \rangle_p = \sum_{j=1}^p \langle f_j, g_j \rangle$ and its associated norm $\|\cdot\|_p$. In this paper, multivariate functional data constitute a random sample from a multivariate process $\{X(t) \in \mathbb{R}^p : t \in [0, 1]\}$, which we assume to be zero-mean and Gaussian such that $X \in (L^2[0, 1])^p$ almost surely and $E\left(\|X\|_p^2\right) < \infty$. The infinite-dimensional nature of

these data makes dimension reduction a prerequisite for any statistical analysis, and we now review the two most commonly used methods of linear dimension reduction for multivariate functional data. We restrict ourselves to linear methods since a main object of the paper is to fit a graphical model as defined by the covariance properties of X .

The first method is ordinary FPCA applied to each component function. For each j , $j = 1, \dots, p$, the probability measure on $L^2[0, 1]$ associated with X_j is uniquely characterized by the covariance kernel $G_{jj}(s, t) = \text{Cov}(X_j(s), X_j(t))$ or, equivalently, the associated integral operator $\mathcal{G}_{jj} : L^2[0, 1] \rightarrow L^2[0, 1]$ given by $\mathcal{G}_{jj}(f)(\cdot) = \int_0^1 G_{jj}(\cdot, t)f(t) dt$. The well-known Karhunen-Loève expansion states that there exists an orthonormal sequence $\{\phi_{jl}\}_{l=1}^\infty$ formed by the eigenfunctions of \mathcal{G}_{jj} such that

$$X_j(t) = \sum_{l=1}^{\infty} \xi_{jl} \phi_{jl}(t), \quad \xi_{jl} = \langle X_j, \phi_{jl} \rangle = \int_0^1 X_j(t) \phi_{jl}(t) dt. \quad (1)$$

A main takeaway from (1) is the equivalence between X_j and the infinite sequence ξ_{jl} of uncorrelated functional principal component scores (FPCs), which satisfy $E(\xi_{jl}) = 0$ and $\text{Var}(\xi_{jl}) = \lambda_{jl}$. Here, λ_{jl} represents the nonincreasing sequence of repeated eigenvalues of \mathcal{G}_{jj} and satisfies $\sum_{l=1}^{\infty} \lambda_{jl} < \infty$. Expansion (1) is optimal in a univariate sense, as truncation of the series retains the maximum amount of variability for each component [14].

A second option is multivariate FPCA (mFPCA, [6]), which is based on the covariance operator $\mathfrak{G} : (L^2[0, 1])^p \rightarrow (L^2[0, 1])^p$ of X , where $\{\mathfrak{G}(g)\}_j = \sum_{k=1}^p \mathcal{G}_{jk}(g_k)$ and $\mathcal{G}_{jk} : L^2[0, 1] \rightarrow L^2[0, 1]$ is the integral operator with kernel $G_{jk}(s, t) = \text{Cov}(X_j(s), X_k(t))$. The multivariate Karhunen-Loève expansion is based on the orthonormal sequence of eigenfunctions $\rho_l \in (L^2[0, 1])^p$ of \mathfrak{G} :

$$X(t) = \sum_{l=1}^{\infty} \langle X, \rho_l \rangle_p \rho_l(t). \quad (2)$$

In this expansion, the multivariate FPCs $\langle X, \rho_l \rangle_p$ form a sequence of uncorrelated random variables, and are optimal in the sense of retaining variability of the multivariate process.

Turning to the goal of estimating a functional graphical model, the conditional dependency structure of X is informally represented by the conditional covariance kernels

$$C_{jk}(s, t) = \text{Cov}(X_j(s), X_k(t) | X_{-(j,k)}), \quad j, k \in V, j \neq k, \quad (3)$$

where $V = \{1, \dots, p\}$ and $X_{-(j,k)}$ is the vector of functions remaining after removing X_j and X_k . If this object is well-defined, the conditional independence graph $G = (V, E)$ corresponding to X is built by requiring $(j, k) \notin E$ if and only if $C_{jk}(s, t) = 0$ for all $s, t \in \mathcal{T}$. [21] utilized univariate FPCA (1) separately for each function, and demonstrated that, if there exists $M < \infty$ such that $\lambda_{jk} = 0$ for $k \geq M$, C_{jk} can be identified with a finite-dimensional precision matrix, thereby reducing the functional problem to an essentially multivariate one. Such a transition from a continuous kernel C_{jk} to a matrix is possible only if the conditioning variable $X_{-(j,k)}$ is finite dimensional. Interestingly, while the Bayesian methodology in [29] provided a more rigorous definition of conditional independence, priors on the covariance \mathfrak{G} were required to concentrate on finite-dimensional subspaces. Such an assumption is unreasonable for most functional data arising in practice, given the complex phenomena they represent. Aside from this consideration, a key practical drawback of univariate FPCA is that the choice of each component's basis is made without regard to the dependencies between components, so that key aspects of the covariance between features can be omitted in the reduction. On the other hand, mFPCA in (2) is useless in terms of fitting a graphical model, since the multivariate FPCs are scalar random variables and cannot be used to estimate conditional dependencies between component functions.

Intuitively, the goal is to combine the strengths of (1) and (2) as follows. Each component function X_j is represented by a sequence of scores obtained by projecting on an orthonormal basis (as in FPCA), where the basis is chosen optimally to retain the variability in the multivariate process (as in mFPCA). Results in Section 3 demonstrate that this can be achieved by applying an assumption of separability to X . Under this assump-

tion, the conditional covariance kernels C_{jk} in (3) are automatically well-defined, and can be identified with a sequence of $p \times p$ covariance matrices, leading to substantial computational advantages.

3 Notions of Separability

The multi-way structure of the data, represented by the discrete and continuous indices $j = 1, \dots, p$ and $t \in [0, 1]$, make modelling difficult, particularly for understanding and estimating conditional independence. When encountering such complex data, structural assumptions can often simplify matters greatly, both in terms of interpretation and computation. In this case, it is desirable to separate the multivariate and functional aspects of the data. Motivated by recent work on dimension reduction and separability for so-called two-way functional data [1, 17, 4], we investigate similar separability notions for multivariate functional data. Recall that \mathfrak{G} is the covariance operator of X with orthonormal eigenfunctions ρ_l , $l \geq 1$, and let \bar{G} denote its kernel. The developments in this section do not require that X be Gaussian.

Definition 1. X is strongly separable if there exist a covariance matrix Δ and a symmetric, nonnegative definite covariance kernel $B \in L^2[0, 1]^2$ such that

$$\bar{G}(s, t) = \Delta B(s, t).$$

Thus, strong separability of X states that its covariance properties factor cleanly into multivariate and functional aspects. Of course, Δ and B are not identifiable in Definition 1, since one can be scaled by a positive constant and the other by its inverse. However, the eigenvectors of Δ , denoted $\{e_j\}_{j=1}^p$, and eigenfunctions of B , denoted $\{\varphi_l\}_{l=1}^\infty$, are unique. As a consequence, the eigenfunctions of \mathfrak{G} are given by the tensor basis $\{e_j \varphi_l : 1 \leq j \leq p, l \in \mathbb{N}\}$, and the scores $\langle X, e_j \varphi_l \rangle_p$, $\langle X, e_k \varphi_m \rangle_p$ are uncorrelated whenever $j \neq k$ or $l \neq m$.

In fact, it is this last property that is most useful from a statistical point of view. As strong separability is a very restrictive assumption, this leads to the following definition of weak separability [17].

Definition 2. X is weakly separable if there exist orthonormal bases $\{e_j\}_{j=1}^p$ and $\{\varphi_l\}_{l=1}^\infty$ of \mathcal{R}^p and $L^2[0, 1]$, respectively, such that the array

$$\{\langle X, e_j \varphi_l \rangle_p : 1 \leq j \leq p, l \in \mathbb{N}\}$$

consists of uncorrelated random variables.

If weak separability holds, it need not be the case that \bar{G} cleanly factor into multivariate and functional components so that $e_j \varphi_l$ are not necessarily eigenfunctions of \mathfrak{G} . However, the following parallel holds (see [17] for a similar result). Define

$$H(s, t) = \sum_{j=1}^p G_{jj}(s, t), \quad \Gamma = \int_0^1 \bar{G}(t, t) dt. \quad (4)$$

Proposition 1. *If X is weakly separable and the eigenvalues of Γ (respectively, H) have multiplicity one, then the orthonormal basis $\{e_j\}_{j=1}^p$ (respectively, $\{\varphi_l\}_{l=1}^\infty$) is unique and consists of the eigenvectors (resp., eigenfunctions) of Γ (resp., H).*

Proof. By weak separability we have $\langle \mathfrak{G}(e_j \varphi_l), e_{j'} \varphi_{l'} \rangle_p = E(\langle X, e_j \varphi_l \rangle_p \langle X, e_{j'} \varphi_{l'} \rangle_p) = 0$ for $(j, l) \neq (j', l')$. Expanding the kernel \bar{G} in the tensor basis $\{e_j \varphi_l : 1 \leq j \leq p, l \in \mathbb{N}\}$,

$$\bar{G}(s, t) = \sum_{j=1}^p \sum_{l=1}^\infty \text{Var}(\langle X, e_j \varphi_l \rangle_p) e_j e_j^\top \varphi_l(s) \varphi_l(t),$$

so that

$$\Gamma = \sum_{j=1}^p \sum_{l=1}^\infty \text{Var}(\langle X, e_j \varphi_l \rangle_p) e_j e_j^\top \int_0^1 \varphi_l^2(t) dt = \sum_{j=1}^p \left(\sum_{l=1}^\infty \text{Var}(\langle X, e_j \varphi_l \rangle_p) \right) e_j e_j^\top$$

Thus, $\{e_j\}_{j=1}^p$ are the eigenvectors of Γ .

On the other hand, if we marginalize $\bar{G}(s, t)$ over $j \in \{1, \dots, p\}$,

$$H(s, t) = \sum_{j=1}^p \text{Cov}(X_j(s), X_j(t)) = \sum_{l=1}^{\infty} \left(\sum_{j=1}^p \text{Var}(\langle X_j, \varphi_l \rangle) \right) \varphi_l(s) \varphi_l(t)$$

we see that $\{\varphi_l\}_{l=1}^{\infty}$ are the eigenfunctions of $\sum_{j=1}^p G_{jj}(s, t)$.

□

The key point of this result is the identifiability of the target dimension reduction spaces. Weak separability implies that the score vectors $(\langle X_1, \varphi_l \rangle, \dots, \langle X_p, \varphi_l \rangle)^\top$ are uncorrelated across l . When X is Gaussian, these vectors become independent Gaussian p -vectors. As we will see, this independence provides the main simplification in the fitting of an FGGM. However, weak separability implies a bit more, specifically that the stochastic processes $\{e_j^\top X(t) : t \in [0, 1]\}$ are independent across j , which is of no particular advantage in our setting. We thus weaken separability even further as follows.

Definition 3. X is partially separable if there exists an orthonormal basis $\{\varphi_l\}_{l=1}^{\infty}$ of $L^2[0, 1]$ such that the random vectors $\theta_l = (\langle X_1, \varphi_l \rangle, \dots, \langle X_p, \varphi_l \rangle)^\top$, $l \in \mathbb{N}$, are mutually uncorrelated.

Similar to weak separability, if partial separability holds, the basis φ_l is unique. This fact allows for simple estimation of the basis φ_l as will be described in Section 5. Additionally, the basis is optimal under a certain fraction of variance explained criterion.

Theorem 1. *Suppose X is partially separable and that the eigenvalues λ_l of the operator $\mathfrak{H} : L^2[0, 1] \rightarrow L^2[0, 1]$ with kernel H are positive and have multiplicity one. Then*

1. *the basis φ_l is unique and consists of the eigenfunctions \mathfrak{H} , and*
2. *for any orthonormal basis $\{\tilde{\varphi}_l\}_{l=1}^{\infty}$ of $L^2[0, 1]$ and any $L \in \mathbb{N}$,*

$$\sum_{l=1}^L \sum_{j=1}^p \text{Var}(\langle X_j, \tilde{\varphi}_l \rangle) \leq \sum_{l=1}^L \sum_{j=1}^p \text{Var}(\theta_{lj}),$$

where the φ_l are ordered by decreasing eigenvalue, with equality if and only if $\text{span}\{\tilde{\varphi}_1, \dots, \tilde{\varphi}_L\} = \text{span}\{\varphi_1, \dots, \varphi_L\}$.

Proof. To see part a), first observe that $X_j(t) = \sum_{l=1}^{\infty} \theta_{lj} \varphi_l(t)$ almost surely, for any φ_l satisfying Definition 3. Let $H(s, t) = \sum_{l=1}^{\infty} \tau_l \eta_l(s) \eta_l(t)$, be the unique Mercer expansion [14], where η_l form an orthonormal sequence in $L^2[0, 1]$ and τ_l is a nonincreasing sequence of positive numbers with $\sum_{l=1}^{\infty} \tau_l < \infty$. But by partial separability,

$$\begin{aligned} H(s, t) &= \sum_{j=1}^p \text{Cov} \left(\sum_{l=1}^{\infty} \theta_{lj} \varphi_l(s), \sum_{l'=1}^{\infty} \theta_{l'j} \varphi_{l'}(t) \right) = \sum_{j=1}^p \sum_{l=1}^{\infty} \text{Var}(\theta_{lj}) \varphi_l(s) \varphi_l(t) \\ &= \sum_{l=1}^{\infty} \left(\sum_{j=1}^p \text{Var}(\theta_{lj}) \right) \varphi_l(s) \varphi_l(t), \end{aligned}$$

implying that $\eta_l = \varphi_l$ for each l . For part b), notice that \mathfrak{H} is a self-adjoint Hilbert-Schmidt operator with eigenvalues $\{\tau_l\}_{l=1}^{\infty}$ and eigenfunctions $\{\varphi_l\}_{l=1}^{\infty}$. Hence, by the Schmidt-Mirsky Theorem we see that, for $L \in \mathbb{N}$ and $\|\cdot\|_{\text{HS}}$ denoting the Hilbert-Schmidt norm, the minimization

$$\min_{\text{rank}(\mathcal{W}^*)=L} \|\mathfrak{H} - \mathcal{W}^*\|_{\text{HS}}^2 = \sum_{l=L+1}^{\infty} \tau_l^2$$

is uniquely attained by the integral operator \mathcal{W} with kernel $W = \sum_{l=1}^L \tau_l \varphi_l(s) \varphi_l(t)$. Therefore, for any orthonormal basis $\{\tilde{\varphi}_l\}_{l=1}^{\infty}$ of $L^2[0, 1]$ we have

$$\sum_{l=1}^L \sum_{j=1}^p \text{Var}(\theta_{lj}) \geq \sum_{l=1}^L \sum_{j=1}^p \text{Var}(\langle X_j, \tilde{\varphi}_l \rangle)$$

with equality if and only if $\text{span}\{\tilde{\varphi}_1, \dots, \tilde{\varphi}_L\} = \text{span}\{\varphi_1, \dots, \varphi_L\}$.

□

4 The Functional Gaussian Graphical Model for Partially Separable Processes

Under the assumption that X is partially separable, the multivariate process X admits an expansion

$$X(t) = \sum_{l=1}^{\infty} \theta_l \varphi_l(t), \quad \theta_{lj} = \int_0^1 X_j(s) \varphi_l(s) ds, \quad (5)$$

dubbed the partial separability Karhunen-Loève expansion (PSKL). We thus refer to φ_l as the PSKL basis. The coefficient vectors $\theta_l = (\theta_{l1}, \dots, \theta_{lp})$ satisfy $\text{Cov}(\theta_{lj}, \theta_{l'k}) = 0$ whenever $l \neq l'$; they are mutually uncorrelated. While the assumption of partial separability can be made independently of Gaussianity, under the assumption of a Gaussian process, this implies that the θ_l are mutually independent Gaussian random vectors. Let $\Sigma_l = (\sigma_{ljk})_{j,k=1}^p = \text{Var}(\theta_l)$, so that $\theta_l \stackrel{\text{ind}}{\sim} \mathcal{N}(0, \Sigma_l)$. For ease of presentation, suppose Σ_l is positive definite for all l .

Recall that, in order to define a coherent FGGM, one needs a well-defined measure of conditional covariance between component functions X_j and X_k , informally described by (3). For any fixed $j, k \in V = \{1, \dots, p\}$, define $V_{jk} = V \setminus \{j, k\}$ and the quantities

$$\begin{aligned} c_{jk} &= (\sigma_{ljm})_{m \in V_{jk}} = \text{Cov}(\theta_{l, -(j,k)}, \theta_{lj}), \\ c_{kj} &= (\sigma_{lkm})_{m \in V_{jk}} = \text{Cov}(\theta_{l, -(j,k)}, \theta_{lk}), \\ \Lambda_{jk} &= (\sigma_{lmm'})_{m, m' \in V_{jk}} = \text{Var}(\theta_{l, -(j,k)}). \end{aligned}$$

Then the conditional covariance between θ_{lj} and θ_{lk} given $\theta_{l, -(j,k)} = (\theta_{lm})_{m \in V_{jk}}$ is

$$\tilde{\sigma}_{ljk} = \sigma_{ljk} - c_{jk}^\top \Lambda_{jk}^{-1} c_{kj}. \quad (6)$$

Since we are dealing with a finite-dimensional model for each θ_l , we also have a connection

between $\tilde{\sigma}_{ljk}$ and the precision matrix $\Omega_l = (\omega_{ljk})_{j,k \in V} = \Sigma_l^{-1}$. Specifically,

$$\tilde{\sigma}_{ljk} = \left[(\Omega_l^{jk})^{-1} \right]_{12}, \quad \Omega_l^{jk} = \begin{pmatrix} \omega_{ljj} & \omega_{ljk} \\ \omega_{lkj} & \omega_{lkk} \end{pmatrix}.$$

The next result establishes that the conditional covariance functions C_{jk} are well-defined when the PSKL expansion holds. The proof of this and all remaining results can be found in the Appendix.

Theorem 2. *If X is partially separable, then, for all $s, t \in [0, 1]$, the covariance between $X_j(s)$ and $X_k(t)$ conditional on the multivariate subprocess $\{X_{-(j,k)}(u) : u \in [0, 1]\}$ is*

$$C_{jk}(s, t) = \sum_{l=1}^{\infty} \tilde{\sigma}_{ljk} \varphi_l(s) \varphi_l(t). \quad (7)$$

Now, the conditional independence graph for the multivariate Gaussian process can be defined by $(j, k) \notin E$ if and only if $C_{jk}(s, t) \equiv 0$. In fact, the edge set E in this partially separable functional Gaussian graphical model (psFGGM) has a direct connection to the finite-dimensional graphs E_l for which $(j, k) \in E_l$ if and only if $\tilde{\sigma}_{ljk} = 0$.

Corollary 1. *Under the setting of Theorem 2, the functional graph edge set E is related to the sequence of edge sets E_l by $E = \bigcup_{l=1}^{\infty} E_l$.*

5 Estimation

The developments of the previous section suggest that, under the assumption of partial separability, the precision matrices $\Omega_l = \Sigma_l^{-1}$ contain all of the conditional independence information about X . In fact, as a consequence of the PSKL expansion, $\text{trace}(\Sigma_l) = \lambda_l \rightarrow 0$, so it is more convenient and stable to work with $\Xi_l = R_l^{-1}$, where R_l is the correlation matrix corresponding to Σ_l . An immediate consequence will be an estimator of the overall edge set,

but Ξ_l contains even richer information beyond the adjacency matrix, such as the coefficients in the conditional covariance functions in (7). After defining the estimation procedure, convergence rates will be established under the setting of fully-observed functional data. This setting is used for simplicity and in order to maintain comparability with [21], who also made this assumption in theoretical developments. Simulations and data analysis will investigate the estimators under discretely and noisily observed functional data.

Consider a sample X_1, \dots, X_n , independently and identically distributed according to a multivariate Gaussian process X . In order to make these methods applicable to any functional data set, it is assumed that one has constructed preliminary estimates $\hat{\mu}_j$ and \hat{G}_{jk} , $j, k = 1, \dots, p$, of the individual mean functions $\mu_j(t) = E(X_j(t))$, $t \in [0, 1]$, and auto- and cross-covariance functions for each component. As an example, if the X_i are fully observed, cross-sectional estimates

$$\hat{\mu}_j(t) = \frac{1}{n} \sum_{i=1}^n X_{ij}(t), \quad \hat{G}_{jk}(s, t) = \frac{1}{n} \sum_{i=1}^n (X_{ij}(s) - \hat{\mu}_j(s))(X_{ik}(t) - \hat{\mu}_k(t)) \quad (8)$$

can be used. For other observational designs, smoothing can be applied to the pooled data to estimate these quantities [26, 25]. Given such preliminary estimates, the kernel H in (4) is estimated by

$$\hat{H}(s, t) = \sum_{j=1}^p \hat{G}_{jj}(s, t),$$

leading to empirical eigenvalue/eigenfunction pairs $(\hat{\lambda}_l, \hat{\varphi}_l)$ as estimates of the PSKL components. These quantities can be used to compute estimates of σ_{ljk} as

$$s_{ljk} = (S_l)_{jk} = \widehat{\text{Cov}}(\langle X_{1j}, \varphi_l \rangle, \langle X_{1k}, \varphi_l \rangle) = \int_{[0,1]^2} \hat{G}_{jk}(s, t) \hat{\varphi}_l(s) \hat{\varphi}_l(t) ds dt. \quad (9)$$

A group graphical lasso approach [8] will be used to estimate the Ξ_l . Let

$$(\hat{R}_l)_{jk} = r_{ljk} = s_{ljk} / [s_{ljj} s_{lkk}]^{1/2}$$

be the estimated correlations. The estimation targets the first L inverse correlation matrices Ξ_l by

$$(\hat{\Xi}_1, \dots, \hat{\Xi}_L) = \underset{\Upsilon_l \succ 0}{\operatorname{argmin}} \sum_{l=1}^L \left\{ \operatorname{trace}(\hat{R}_l \Upsilon_l) - \log(|\Upsilon_l|) \right\} + P(\Upsilon_1, \dots, \Upsilon_L), \quad (10)$$

This corresponds to a penalized likelihood objective function under the Gaussian assumption on the X_i , where the penalty function is

$$P(\Upsilon_1, \dots, \Upsilon_L) = \gamma \left[\alpha \sum_{l=1}^L \sum_{j \neq k} |v_{ljk}| + (1 - \alpha) \sum_{j \neq k} \sqrt{\sum_{l=1}^L v_{ljk}^2} \right], \quad (\Upsilon_l)_{jk} = v_{ljk}. \quad (11)$$

The parameters $\gamma > 0$ and $\alpha \in [0, 1]$ control the overall sparsity level and common sparsity pattern, respectively, in the estimates $\hat{\Xi}_l$, although we have suppressed this dependence in our notation. Then the estimated edge set is $(j, k) \in \hat{E}_l$ if and only if $\hat{\omega}_{ljk} \neq 0$. Although the joint graphical lasso estimator in [8] was proposed for borrowing structural information across multiple classes of multivariate data, it is utilized here for a slightly different purpose. Due to the equality $E = \bigcup_{l=1}^{\infty} E_l$, inducing a common sparsity pattern in the precision matrix estimates intuitively causes the most prominent edges, those that appear in many different sets E_l , to be included in the estimated graph $\hat{E} = \bigcup_{l=1}^L \hat{E}_l$. Lastly, letting $\hat{\Gamma}_l$ be the diagonal matrix of scale estimates $s_{ljj}^{1/2}$, one immediately obtains estimates $\hat{\Omega}_l = \hat{\Gamma}_l^{-1} \hat{\Xi}_l \hat{\Gamma}_l^{-1}$ and $\hat{\Sigma}_l = \hat{\Omega}_l^{-1}$.

The main consistency result considers joint estimation of the matrices Ξ_l under the setting of fully observed functional data, so that $\hat{\mu}$ and \hat{G}_{jk} are as in (8), and with $\alpha = 1$ in (11), corresponding to a strict graphical lasso penalty. As a preliminary result, we first derive a concentration inequality for the estimated covariances s_{ljk} in (9), requiring the following mild assumption.

(A1) The eigenvalues $\lambda_l = \operatorname{trace}(\Sigma_l)$ are distinct, and thus strictly decreasing.

The eigenvalue spacings play a key role in the first theorem through the quantities $\tau_1 =$

$2\sqrt{2}(\lambda_1 - \lambda_2)^{-1}$ and

$$\tau_l = 2\sqrt{2} \max \{ (\lambda_{l-1} - \lambda_l)^{-1}, (\lambda_l - \lambda_{l+1})^{-1} \}, \quad l \geq 2.$$

Set $d_L = \min_{l=1, \dots, L} \tau_l$.

Theorem 3. *Suppose that X is a partially separable Gaussian process and that (A1) holds. Then there exist constants $C_1, C_2 > 0$ such that, for any $0 < \delta \leq C_1$ and for all $l = 1, \dots, L$ and $j, k = 1, \dots, p$,*

$$P(|s_{ljk} - \sigma_{ljk}| \geq \delta) \leq C_2 \exp \{ -C_1 d_L^{-2} n \delta^2 \}. \quad (12)$$

A similar result was obtained by [21] under much stricter assumptions. As a comparison, if we simply add the assumption that $d_L = O(L^{1+\beta})$ for some $\beta > 1$, then for any $0 < \alpha < 1/(4\beta)$, the choice $L = n^\alpha$ yields

$$P(|s_{ljk} - \sigma_{ljk}| \geq \delta) \leq C_2 \exp \left\{ -C_1 n^{1-2\alpha(1+\beta)} \delta^2 \right\}.$$

Additionally, our method of proof is greatly simplified by using the inequality

$$|s_{ljk} - \sigma_{ljk}| \leq 2\tau_l \|G_{jk}\|_{[0,1]^2} \|\hat{H} - H\|_{[0,1]^2} + \|\hat{G}_{jk} - G_{jk}\|_{[0,1]^2},$$

where $\|\cdot\|_{[0,1]^2}$ is the usual $L^2[0,1]^2$ norm. Because the estimator targets the inverse correlation matrices, the following corollary is useful. Let $\underline{\sigma}_l = \min_j \sigma_{ljj}$ and $\pi_L = \min_{l=1, \dots, L} \underline{\sigma}_l$.

Corollary 2. *Under the setting of Theorem 3, there exist $C_1, C_2 > 0$ such that for any $0 < \delta \leq C_1$ and all $l = 1, \dots, L$, $j, k = 1, \dots, p$, $j \neq k$,*

$$P(|\hat{r}_{ljk} - r_{ljk}| \geq \delta) \leq C_2 \exp \{ -C_1 d_L^{-2} \pi_L^2 n \delta^2 \}.$$

Finally, applying this concentration result to the estimators in the usual way, a joint rate of convergence is obtained for the first L inverse correlation estimates $\hat{\Xi}_l$, $l = 1, \dots, L$, where L diverges with n . This requires one additional assumption.

(A2) The condition numbers of R_l are uniformly bounded above.

Let $\|\cdot\|_F$ denote the matrix Frobenius norm and write $|E_l|$ for the number of elements (edge pairs) in E_l .

Theorem 4. *Suppose assumptions (A1) and (A2) hold, and define $q_L = \left[\sum_{l=1}^L |E_l|\right]^{1/2}$. If $L = L(n)$ satisfies $q_L^{1/2} d_L \pi_L^{-1} = o(n^{1/2})$ and $\gamma \asymp \frac{d_L}{n^{1/2} \pi_L}$, then*

$$\sum_{l=1}^L \|\hat{\Xi}_l - \Xi_l\|_F^2 = O_p\left(\frac{d_L^2 q_L}{n \pi_L^2}\right) = o_p(1).$$

For example, if the edge sets are eventually empty so that $q_L = O(1)$, and if $d_L/\pi_L = O(L^\beta)$, $\beta > 1$, grows at a polynomial rate, then the choices $L = n^\alpha$ and $\gamma \asymp n^{\alpha\beta-1/2}$ for $2\alpha\beta < 1$ yield a rate of $n^{2\alpha\beta-1}$ for $\sum_{l=1}^L \|\hat{\Xi}_l - \Xi_l\|_F^2$.

6 Numerical Experiments

We perform extensive simulation studies in this section comparing psFGGM with the FGGM of [21]. Other potentially competing non-functional based approaches are not included since they are clearly outperformed by FGGM (see [21]).

6.1 Simulation Setup

All settings start with a conditional independence graph $G = (V, E)$ with nodes $V = \{1, \dots, p\}$ and edge set E . The graph is generated from a power law distribution with parameter $\pi = P((i, j) \in E)$. Then, for a fixed M , a sequence of edge sets E_1, \dots, E_M is generated so that $E = \bigcup_{l=1}^M E_l$. This process has two main steps. First, a set of common edges to all edge sets is computed and denoted as E_c for a given proportion of common edges $\tau \in [0, 1]$. Next, the set of edges $E \setminus E_c$ is partitioned into $\tilde{E}_1, \dots, \tilde{E}_M$ where $|\tilde{E}_l| \geq |\tilde{E}_{l'}|$

for $l < l'$ and set $E_l = E_c \cup \tilde{E}_l$. More details for constructing E_1, \dots, E_M can be found in the Appendix.

Next, one $p \times p$ precision matrix Ω_l for each E_l is generated following the algorithm in [18]. Let $\tilde{\Omega}_l$ be a $p \times p$ matrix with entries:

$$\tilde{\Omega}_l(i, j) = \begin{cases} 1 & \text{if } i = j \\ 0 & \text{if } (i, j) \notin E_l \text{ or } i < j \\ \sim \mathcal{U}(\mathcal{D}) & \text{if } (i, j) \in E_l \end{cases}$$

where $\mathcal{D} = [-2/3, -1/3] \cup [1/3, 2/3]$. And finally, $\tilde{\Omega}_l$ is rescaled by rows, averaged with its transpose and has its diagonal entries set to one. This process outputs a precision matrix Ω_l which is guaranteed to be symmetric and diagonally dominant.

Then, one can sample $\boldsymbol{\theta}_i = (\theta_{i1}, \dots, \theta_{iM})^\top \in \mathbb{R}^{Mp}$ with $\theta_{il} = (\theta_{il1}, \dots, \theta_{ilp})^\top \in \mathbb{R}^p$ for $i = 1, \dots, n$ from a mean zero multivariate normal distribution. For the $Mp \times Mp$ covariance matrix Σ we consider two models, Σ_{ps} and $\Sigma_{\text{non-ps}}$, corresponding to partially separable and non-partially separable X , respectively:

- (i) Partially separable case: $\Sigma_{\text{ps}} = \text{diag}(\Sigma_1, \dots, \Sigma_M)$ with $\Sigma_l = a_l \Omega_l^{-1}$ and decaying factors $a_l = 3l^{-1.8}$. This guarantees that $\text{trace}(\Sigma_l)$ decreases monotonically on l and that Σ_{ps} satisfies the assumptions of a partially separable multivariate Gaussian process.
- (ii) Non-partially separable case: A block-banded precision matrix Ω is computed with $p \times p$ blocks $\Omega_{l,l} = \Omega_l$ and $\Omega_{l+1,l} = \Omega_{l,l+1} = 0.5(\Omega_l^* + \Omega_{l+1}^*)$ with $\Omega_l^* = \Omega_l - \text{diag}(\Omega_l)$. This ensures that Ω is positive definite with non-zero off-diagonal blocks breaking the partial separability assumptions. Next, one computes a covariance matrix

$$\Sigma_{\text{non-ps}} = \text{diag}(\Sigma_{\text{ps}})^{\frac{1}{2}} \left(\text{diag}(\Omega)^{-\frac{1}{2}} \Omega \text{diag}(\Omega)^{-\frac{1}{2}} \right)^{-1} \text{diag}(\Sigma_{\text{ps}})^{\frac{1}{2}}$$

with Σ_{ps} as in (i).

Finally, discrete and noisy functional data were generated as

$$Y_{ijk} = X_{ij}(t_k) + \varepsilon_{ijk}, \quad \varepsilon_{ijk} \sim N(0, \sigma_\varepsilon^2),$$

with $\sigma_\varepsilon^2 = 0.05 \frac{\sum_{l=1}^M \text{trace}(\Sigma_l)}{p}$ and $X_{ij}(t_k) = \sum_{l=1}^M \theta_{ilj} \varphi_l(t_k)$ generated according to the PSKL expansion in (5), $i = 1, \dots, n$ and $j = 1, \dots, p$. Fourier basis functions $\varphi_1, \dots, \varphi_M$ evaluated on an equally spaced time grid of t_1, \dots, t_T , with $t_1 = 0$ and $t_T = 1$, were used to generate the data. In all settings, 100 simulations were conducted. To resemble real fMRI data from the HCP, we set $T = 30$, $M = 20$ and $\pi = 5\%$ for a sparse graph.

6.2 Comparison Results

We compare our method psFGGM against the FGGM, which we estimate using the code provided by the authors [21]. As performance metrics, the true positive rate (TPR) and false positive rate (FPR) of correctly identifying edges in graph G are computed varying γ for a fixed value of α . The latter parameter takes values in a coarse grid of five evenly spaced points spanning the interval $[0,1]$, and the value maximizing the area under the ROC curve is considered for the comparison. In all cases, a power law distribution parameter $\pi = 0.05$ and a proportion of common edges $\tau = 0$ were used.

The two methods are compared using L principal components explaining at least 90% of the variance. For all simulations, this threshold results in the choice of $L = 5$ or $L = 6$ components for both FGGM and psFGGM. For higher thresholds requiring larger values of L , however, we see a sharp contrast; while psFGGM consistently converges to a solution, FGGM does not, due to increasing numerical instability. The likely reason for the instability of FGGM is due to the fact that it requires estimation of $\mathcal{O}(L^2 p^2)$ free parameters. On the other hand, psFGGM estimates a precision matrix with $\mathcal{O}(L p^2)$ free parameters. In this sense, psFGGM estimator effectively regularizes the solution more, leading to numerical stability. As a result, psFGGM is able to include more functional bases into the analysis,

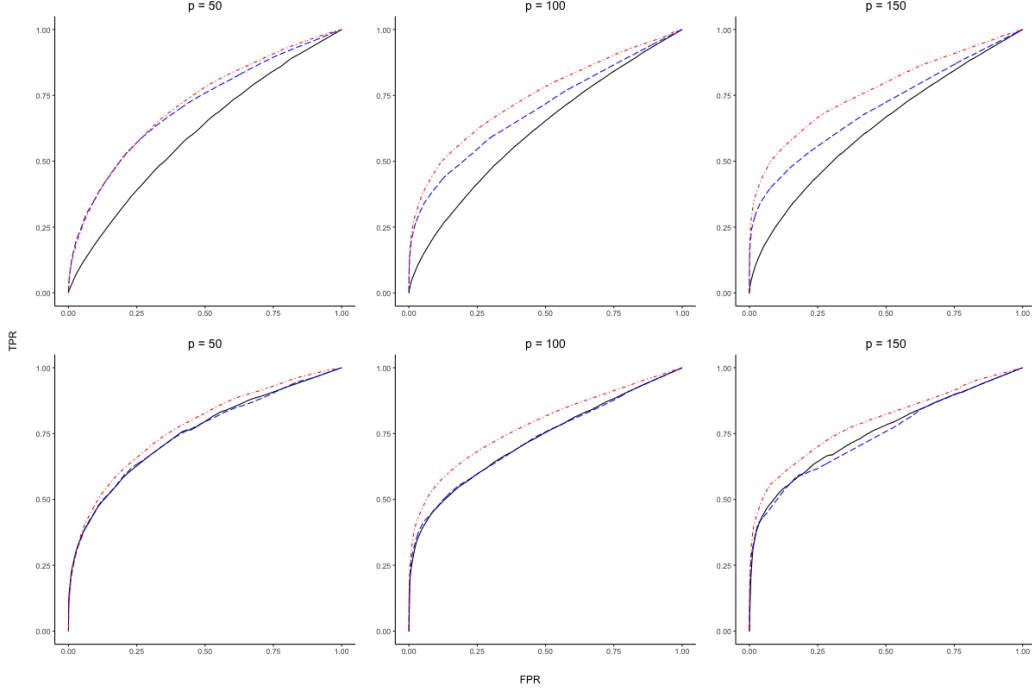


Figure 1: Mean ROC curves for $psFGGM$ and $FGGM$ under Σ_{ps} (top) and Σ_{non-ps} (bottom) for $p = 50, 100, 150$ and $n = p/2$. We see $psFGGM$ (---) and $FGGM$ (—) at 90% of variance and $psFGGM$ (-.-) at 95% of variance explained.

thereby incorporating more information from the data. In the figures and tables, additional results are available for $psFGGM$ when L is increased to explain at least 95% of the variance.

Figure 1 shows average ROC curves for the high-dimensional case with $n = p/2$. The smoothed curves are computed using the `supsmu` R package that implements SuperSmoother [10], a variable bandwidth smoother that uses cross-validation to find the best bandwidth. Table 1 shows the mean and standard deviation of area under the ROC curves estimates under various simulation settings. When the partial separability assumption is satisfied, i.e., $\Sigma = \Sigma_{ps}$, $psFGGM$ exhibits uniformly higher TPR profile across the FPR range. Even when the partial separability assumption is not satisfied, i.e., $\Sigma = \Sigma_{non-ps}$, $psFGGM$ and

Table 1: Mean AUC (standard error) values for Figure 1

Σ	p	AUC			AUC15 [†]		
		FGGM _{90%}	psFGGM _{90%}	psFGGM _{95%}	FGGM _{90%}	psFGGM _{90%}	psFGGM _{95%}
Σ_{ps}	50	0.60(0.03)	0.71(0.04)	0.72(0.04)	0.15(0.04)	0.30(0.05)	0.29(0.05)
Σ_{ps}	100	0.62(0.02)	0.69(0.02)	0.74(0.02)	0.18(0.02)	0.35(0.02)	0.40(0.03)
Σ_{ps}	150	0.63(0.01)	0.70(0.01)	0.77(0.02)	0.20(0.01)	0.37(0.02)	0.46(0.03)
$\Sigma_{\text{non-ps}}$	50	0.75(0.03)	0.75(0.03)	0.77(0.03)	0.39(0.04)	0.39(0.04)	0.41(0.05)
$\Sigma_{\text{non-ps}}$	100	0.72(0.02)	0.73(0.02)	0.78(0.02)	0.40(0.02)	0.42(0.03)	0.48(0.03)
$\Sigma_{\text{non-ps}}$	150	0.75(0.02)	0.74(0.03)	0.79(0.02)	0.45(0.03)	0.44(0.04)	0.51(0.03)

[†]AUC15 is AUC computed for FPR in the interval $[0, 0.15]$, normalized to have maximum area 1.

FGGM perform comparably. More importantly and in all cases, psFGGM is able to leverage 95% level of variance explained, owing to the numerical stability mentioned above. Figure 2 and Table 2 summarize results for the large sample case $n = 1.5p$ with similar conclusions.

A comparison of the two methods under a the very sparse case is also considered. For this case one has $\pi = 0.025$ with a proportion of common edges $\tau = 0$. Finally, we check the robustness of our conclusions under other settings including $\tau \in \{0, 0.1, 0.2\}$ and $\pi \in \{2.5\%, 5\%, 10\%\}$, as well as p greater, equal or smaller than n . Results for a very sparse case with $\pi = 0.025$ are included in the Appendix. All simulation experiments show a comparative advantage of psFGGM.

7 Application to Functional Brain Connectivity

In this section, psFGGM is used to reconstruct the functional brain connectivity structure using functional magnetic resonance imaging (fMRI) data from the Human Connectome Project (HCP). We analyze the ICA-FIX preprocessed data variant as suggested by [11] that controls for spatial distortions and alignments across both subjects and modalities.

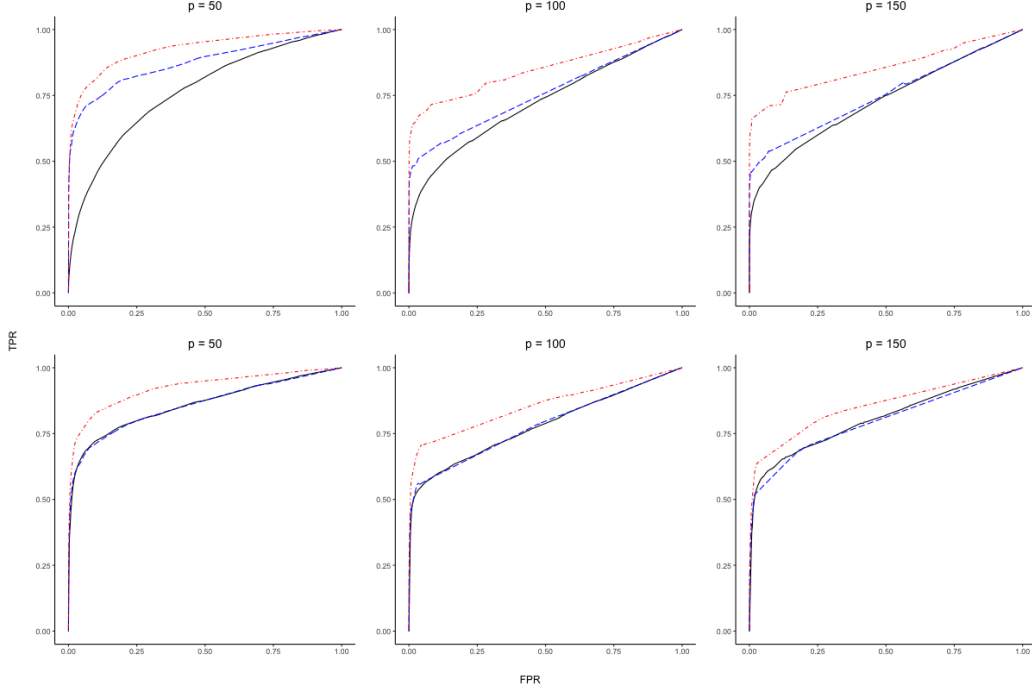


Figure 2: Mean ROC curves for $psFGGM$ and $FGGM$ under Σ_{ps} (top) and Σ_{non-ps} (bottom) for $p = 50, 100, 150$ and $n = 1.5p$. We see $psFGGM$ (---) and $FGGM$ (—) at 90% of variance and $psFGGM$ (-.-) at 95% of variance explained.

In this work, the goal is to reconstruct the connectivity pattern between 360 cortical regions of interest (ROIs) given in [12] using $psFGGM$ approach. Each ROI timeseries signal is obtained by averaging all BOLD signals from the ROI.

For the analysis, we use the motor task fMRI dataset¹. This dataset consists of fMRI scans of individuals performing basic body movements. During each scan, a sequence of visual cues signals the subject to move one of five body parts: fingers of the left or right hand; toes of the left or right foot; or the tongue. After each three-second cue, a body movement lasts for 12 seconds with temporal resolution of 0.72 seconds.

¹The 1200 Subjects 3T MR imaging data available at <https://db.humanconnectome.org>

Table 2: Mean AUC (standard error) values for Figure 2

Σ	p	AUC			AUC15 [†]		
		FGGM _{90%}	psFGGM _{90%}	psFGGM _{95%}	FGGM _{90%}	psFGGM _{90%}	psFGGM _{95%}
Σ_{ps}	50	0.76(0.02)	0.87(0.03)	0.92(0.02)	0.37(0.04)	0.69(0.04)	0.75(0.04)
Σ_{ps}	100	0.72(0.02)	0.75(0.02)	0.84(0.02)	0.41(0.02)	0.52(0.02)	0.68(0.03)
Σ_{ps}	150	0.73(0.01)	0.75(0.01)	0.85(0.02)	0.44(0.02)	0.52(0.02)	0.69(0.03)
$\Sigma_{\text{non-ps}}$	50	0.86(0.02)	0.85(0.02)	0.92(0.03)	0.66(0.03)	0.65(0.04)	0.76(0.06)
$\Sigma_{\text{non-ps}}$	100	0.78(0.02)	0.78(0.02)	0.85(0.02)	0.55(0.03)	0.56(0.04)	0.68(0.03)
$\Sigma_{\text{non-ps}}$	150	0.80(0.03)	0.79(0.03)	0.85(0.02)	0.57(0.04)	0.55(0.05)	0.64(0.03)

[†]AUC15 is AUC computed for FPR in the interval $[0, 0.15]$, normalized to have maximum area 1.

The left- and right-hand tasks are analyzed separately. Both of them consider the same $n = 1054$ subjects with complete records and $p = 360$ ROIs. Having removed cool down and ramp up observations, we end up with $T = 16$ time points of pure movement tasks. For illustration purposes, we use penalty parameters $\gamma = 0.91$ and $\alpha = 0.95$ to estimate very sparse graphs in both cases.

Figure 3 shows comparison of activation patterns from left and right-hand task datasets. We visualize the resulting ROI graph on a flat brain map by coloring those ROIs which have any positive degree of connectivity. Connected ROIs that are unique to each task (Figures 3a and 3b on top) are distinguished from those that are common to both (Figure 3c). One can see that almost all of the visual cortex ROIs in the occipital lobe are shared by both maps. This is expected as both tasks require individuals to watch visual cues. On the other hand, the main difference between these motor tasks lies at the motor cortex near the central sulcus. In Figure 3a and 3b the functional maps for the left- and right-hand tasks present particular motor-related cortical areas in the right and left hemisphere, respectively. These results are in line with the motor task activation maps obtained by [2].

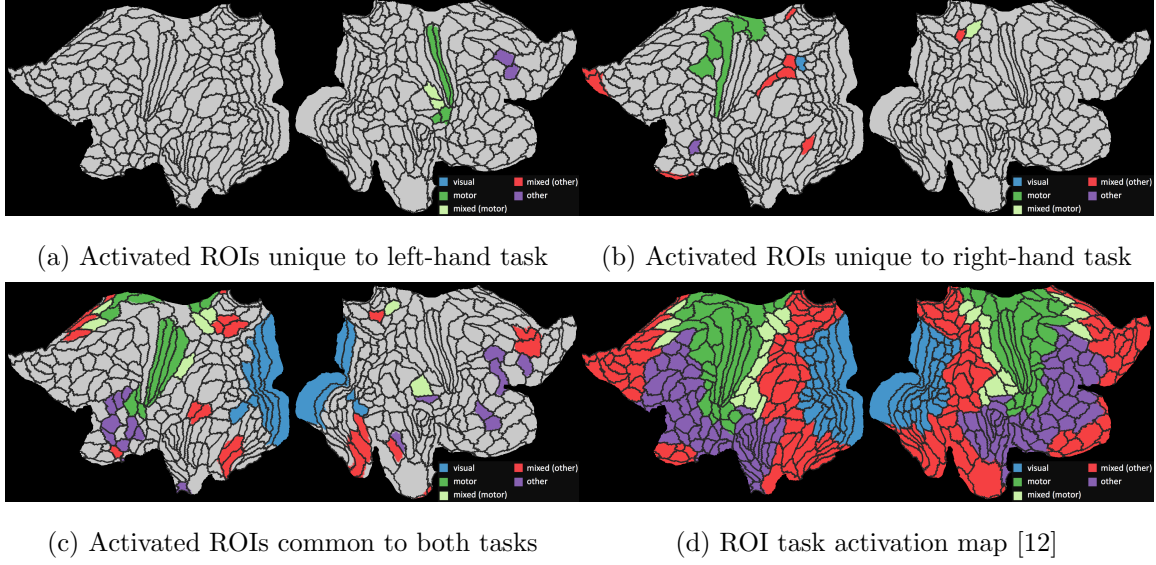


Figure 3: *psFGGM* estimated functionally connected cortical ROIs for the left- and right-hand motor tasks. Each sub-figure shows a flat brain map of the left and right hemispheres (in that order). ROIs having a positive degree of connectivity in each estimated graph are colored based on their functionality [12]: visual (*blue*), motor (*green*), mixed motor (*light green*), mixed other (*red*) and other (*purple*).

8 Discussion

Partial separability for multivariate functional data is a novel structural assumption with further potential applications beyond graphical models. For example, it is well-known that the functional linear model (see [24] and references therein) can be simplified by univariate FPCA, which parses out the problem into a sequence of univariate regressions. The PSKL expansion in (5) demonstrates a similar potential, namely to break down a problem involving multivariate functional data into a sequence of standard multivariate problems. This potential was demonstrated in this paper by decomposing a functional

graphical model into a sequence of standard multivariate graphical models.

We have presented partial separability for multivariate processes X where each component X_j is a function defined on the same domain, motivated by the brain connectivity example. However, this restriction is not strictly necessary in order to define partial separability. If X_j are elements of $L^2(\mathcal{T}_j)$, $j = 1, \dots, p$, a more general definition of partial separability would be the existence of orthonormal bases $\{\varphi_{jl}\}_{l=1}^\infty$ of $L^2(\mathcal{T}_j)$, $j = 1, \dots, p$, such that the vectors $\theta_l = (\theta_{l1}, \dots, \theta_{lp})^\top$, where $\theta_{lj} = \int_{\mathcal{T}_j} X_j(t) \varphi_{jl}(t) dt$ are mutually uncorrelated across l . Such a generalization is highly desirable, as many multivariate functional data sets consist of functions on different domains. In fact, the above notion is even applicable when the domains \mathcal{T}_j are of different dimension [13] or even a complex manifold, such as the surface of the brain. Questions of uniqueness and optimality of the bases φ_{jl} are promising areas of future research.

The psFGGM is equally applicable to dense or sparse functional data, observed with or without noise. However, rates of convergence will inevitably suffer as observations become more sparse or are contaminated with higher levels of noise. To the best of our knowledge, concentration results such as Theorem 3 of this paper or Theorem 1 of [21] are only known for the case of fully observed functional data. Further investigation into graphical models for functional data may yield interesting insights into regime divisions similar to those found by [27].

Appendix

This section contains proofs of the theoretical results in 4 and 5 and one additional auxiliary result. We also give details on the algorithm used in Section 6 to generate a sequence of edge sets (one per basis function) having a given proportion of common edges. Lastly, we provide ROC curves and performance metrics for additional simulation settings.

Proofs of Results from Section 4

Proof of Theorem 2. We have

$$\begin{aligned}
& \text{Cov}(X_j(s), X_k(t) | \{X_{-(j,k)}(u) : u \in (0, 1)\}) \\
&= \text{Cov} \left(\sum_{l=1}^{\infty} \theta_{lj} \varphi_l(s), \sum_{l'=1}^{\infty} \theta_{l'k} \varphi_{l'}(t) | \{X_{-(j,k)}(u) : u \in (0, 1)\} \right) \\
&= \sum_{l,l'=1}^{\infty} \text{Cov}(\theta_{lj}, \theta_{l'k} | \{X_{-(j,k)}(u) : u \in (0, 1)\}) \varphi_l(s) \varphi_{l'}(t) \\
&= \sum_{l=1}^{\infty} \text{Cov}(\theta_{lj}, \theta_{lk} | \{\theta_{l,-(j,k)}\}) \varphi_l(s) \varphi_l(t) \\
&= \sum_{l=1}^{\infty} \tilde{\sigma}_{ljk} \varphi_l(s) \varphi_l(t)
\end{aligned}$$

Convergence of the sum in the last line follows from the fact that $|\tilde{\sigma}_{ljk}| \leq \max_{j=1,\dots,p} \sigma_{ljj}$, so that, for $C = \sup_l \max_j \sigma_{ljj} < \infty$,

$$\sum_{l=1}^{\infty} \tilde{\sigma}_{ljk}^2 \leq \sum_{j=1}^p \sum_{l=1}^{\infty} \sigma_{ljj}^2 \leq C \sum_{j=1}^p \sum_{l=1}^{\infty} \sigma_{ljj} = C \sum_{j=1}^p E(\|X_j\|^2) < \infty.$$

□

Proofs of Results from Section 5

Lemma 1. *Let $\{X(t) \in \mathbb{R}^p : t \in [0, 1]\}$ be a partially separable multivariate Gaussian process such that $E(\|X_j\|^2) < \infty$, $j = 1, \dots, p$, and let $\hat{\mu}_j$ and \hat{G}_{jk} , $j, k = 1, \dots, p$, be the mean and covariance estimates in (8) for a sample of fully observed functional data $X_i \sim X$. Then there exist constants $C_1, C_2 > 0$ such that, for any $0 < \delta \leq C_1$ and for all $j, k = 1, \dots, p$,*

$$P\left(\|\hat{G}_{jk} - G_{jk}\|_{[0,1]^2} \geq \delta\right) \leq C_2 \exp\{-C_1 n \delta^2\}.$$

Proof. Since there are only finitely many pairs (j, k) , we will show the existence of C_1, C_2 for an arbitrary pair which will imply the result. Without loss of generality, assume $\mu_j(t) = E(X_{1j}(t)) \equiv 0$ and set $Y_{ijk}(s, t) = X_{ij}(s)X_{ik}(t)$, $\bar{Y}_{jk} = n^{-1} \sum_{i=1}^n Y_{ijk}$. Then the triangle inequality implies

$$P\left(\|\hat{G}_{jk} - G_{jk}\|_{[0,1]^2} \geq \delta\right) \leq P\left(\|\bar{Y}_{jk} - G_{jk}\|_{[0,1]^2} \geq \frac{\delta}{2}\right) + 2 \max_j P\left(\|\hat{\mu}_j\|^2 \geq \frac{\delta}{2}\right). \quad (13)$$

We begin with the first term on the right-hand side of (13), and will apply Theorem 2.5 of [3]. Since $E(Y_{ijk}(s, t)) = G_{jk}(s, t)$, we need to find $L_1, L_2 > 0$ such that

$$E\left[\|Y_{ijk}(s, t) - G_{jk}(s, t)\|_{[0,1]^2}^b\right] \leq \frac{b!}{2} L_1 L_2^{b-2}, \quad b = 2, 3, \dots,$$

which will then imply that

$$P\left(\|\bar{Y}_{jk} - G_{jk}\|_{[0,1]^2} \geq \frac{\delta}{2}\right) \leq 2 \exp\left\{-\frac{n \delta^2}{8L_1 + 4L_2 \delta}\right\}. \quad (14)$$

Let $M_j = \sum_{l=1}^{\infty} \sigma_{lj} < \infty$ and write $X_j(t) = \sum_{l=1}^{\infty} \sigma_{lj}^{1/2} \xi_{lj} \varphi_l(t)$, where ξ_{lj} are standard normal random variables, independent across i and l . Then, for any $b = 2, 3, \dots$, by Jensen's

inequality,

$$\begin{aligned}
\|Y_{ijk} - G_{jk}\|_{[0,1]^2}^b &= \left(\sum_{l,l'=1}^{\infty} \sigma_{ljj} \sigma_{l'kk} [\xi_{ilj} \xi_{il'k} - \delta_{ll'} r_{ljk}]^2 \right)^{b/2} \\
&= (M_j M_k)^{b/2} \left(\sum_{l,l'=1}^{\infty} \frac{\sigma_{ljj} \sigma_{l'kk}}{M_j M_k} [\xi_{ilj} \xi_{il'k} - \delta_{ll'} r_{ljk}]^2 \right)^{b/2} \\
&\leq (M_j M_k)^{b/2-1} \sum_{l,l'=1}^{\infty} \sigma_{ljj} \sigma_{l'kk} |\xi_{ilj} \xi_{il'k} - \delta_{ll'} r_{ljk}|^b,
\end{aligned}$$

where $\delta_{ll'}$ is the Kronecker delta. The fact that $|r_{ljk}| < 1$ combined with the C_r inequality implies that

$$\sup_{l,l'} E(|\xi_{ilj} \xi_{il'k} - \delta_{ll'} r_{ljk}|) \leq 2^{b-1} \sup_l [E(|\xi_{ilj}|^{2b}) + 1] \leq 2^{b-1} (2^b b! + 1).$$

Thus, with $M = \max_j M_j < \infty$,

$$E\left(\|Y_{ijk} - G_{jk}\|_{[0,1]^2}^b\right) \leq \frac{b!}{2} 2(4M)^{b-2} (4M)^2,$$

and we can take $L_2 = 4M$ and $L_1 = 2L_2^2$ in (14).

By similar reasoning, we can find constants $\tilde{L}_1, \tilde{L}_2 > 0$ such that

$$E(\|X_{1j}\|^b) \leq \frac{b!}{2} \tilde{L}_1 \tilde{L}_2^{b-2}, \quad b = 2, 3, \dots,$$

whence

$$P\left(\|\hat{\mu}_j\|^2 \geq \frac{\delta}{2}\right) \leq 2 \exp\left\{-\frac{n\delta}{4\tilde{L}_1 + 2\tilde{L}_2\sqrt{2\delta}}\right\} \quad (15)$$

Combining (14) and (15), the proof is finished. \square

Proof of Theorem 3. Let \mathcal{G}_{jk} (respectively, $\hat{\mathcal{G}}_{jk}$) be the operator with kernel G_{jk} (resp., \hat{G}_{jk}). Then

$$\sigma_{ljk} = \int_{[0,1]^2} G_{jk}(s, t) \varphi_l(s) \varphi_l(t) ds dt = \langle \mathcal{G}_{jk}(\varphi_l), \varphi_l \rangle$$

and, similarly, $s_{ljk} = \langle \hat{\mathcal{G}}_{jk}(\hat{\varphi}_l), \hat{\varphi}_l \rangle$. Thus, by Lemma 4.3 of [3],

$$\begin{aligned}
|s_{ljk} - \sigma_{ljk}| &\leq |\langle \mathcal{G}_{jk}(\varphi_l), \varphi_l - \hat{\varphi}_l \rangle| + |\langle \mathcal{G}_{jk}(\varphi_l - \hat{\varphi}_l), \hat{\varphi}_l \rangle| + |\langle [\mathcal{G}_{jk} - \hat{\mathcal{G}}_{jk}](\hat{\varphi}_l), \hat{\varphi}_l \rangle| \\
&\leq \|\mathcal{G}_{jk}(\varphi_l)\| \|\varphi_l - \hat{\varphi}_l\| + \|\mathcal{G}_{jk}(\varphi_l - \hat{\varphi}_l)\| \|\hat{\varphi}_l\| + \|[\mathcal{G}_{jk} - \hat{\mathcal{G}}_{jk}](\hat{\varphi}_l)\| \|\hat{\varphi}_l\| \\
&\leq 2\tau_l \|G_{jk}\|_{[0,1]^2} \|\hat{H} - H\|_{[0,1]^2} + \|\hat{G}_{jk} - G_{jk}\|_{[0,1]^2}.
\end{aligned} \tag{16}$$

Now, by applying Lemma 1, there exist $C_1, C_2 > 0$ such that, for all $0 < \delta \leq C_1$ and any $l = 1, \dots, L$ and $j, k = 1, \dots, p$,

$$P(|s_{ljk} - \sigma_{ljk}| \geq \delta) \leq C_2 \exp\{-C_1 d_L^{-2} n \delta^2\}.$$

□

Proof of Corollary 2. Define $\hat{c}_{lj} = \sqrt{s_{ljj}/\sigma_{ljj}}$ and, for $\epsilon > 0$, the events

$$A_l(\epsilon) = \left\{ \max_{j=1, \dots, p} |1 - \hat{c}_{lj}| \leq \epsilon \right\}.$$

Now, fix $\epsilon \in (0, 1)$ and consider $0 < \delta \leq \epsilon$. Then

$$\begin{aligned}
P(|\hat{r}_{ljk} - r_{ljk}| \geq 2\delta) &\leq P(A_l(\epsilon)^c) + P(A_l(\epsilon) \cap \{|\hat{r}_{ljk} - r_{ljk}| \geq 2\delta\}) \\
&\leq P(A_l(\epsilon)^c) + P\left(A_l(\epsilon) \cap \left\{ \frac{1}{\sigma_{ljj}^{1/2} \sigma_{lkk}^{1/2} \hat{c}_{lj} \hat{c}_{lk}} |s_{ljk} - \sigma_{ljk}| \geq \delta \right\}\right) \\
&\quad + P(A_l(\epsilon) \cap \{|\hat{r}_{ljk} - r_{ljk}| \geq 2\delta\}) \\
&\leq P(A_l(\epsilon)^c) + P(|s_{ljk} - \sigma_{ljk}| \geq \delta(1-a)^2 \underline{\sigma}_l) \\
&\quad + P(|1 - \hat{c}_{lj} \hat{c}_{lk}| \geq \delta(1-a)^2).
\end{aligned}$$

We next obtain bounds for the first and last terms of the last line above.

First, since $\delta \leq \epsilon$,

$$P(A_l(\epsilon)^c) \leq p \max_j P(|1 - \hat{c}_{lj}^2| \geq \epsilon) \leq p \max_j P(|s_{ljj} - \sigma_{ljj}| \geq \delta \underline{\sigma}_l).$$

Next, for any $a, b > 0$ such that $|1 - ab| \geq 3\epsilon$, we must have either $|1 - a| \geq \epsilon$ or $|1 - b| \geq \epsilon$. As $\delta < \epsilon < 1$, we have that $\epsilon' = \delta(1 - \epsilon)^2 < 1$ so that

$$P(|1 - \hat{c}_{lj}\hat{c}_{lk}| \geq \delta(1 - \epsilon)^2) \leq P(A_l(\epsilon'/3)^c) \leq p \max_j P\left(|s_{lj} - \sigma_{lj}| \geq \frac{\epsilon'\sigma_l}{3}\right).$$

Putting these together, there exist constants $B_1, B_2 > 0$, independent of j, k, l such that

$$P(|\hat{r}_{ljk} - r_{ljk}| \geq 2\delta) \leq B_2 \max_{l=1,\dots,L} \max_{j,k=1,\dots,p} P(|s_{ljk} - \sigma_{ljk}| \geq B_1\delta\pi_L),$$

so that the result follows from Lemma 3. \square

Proof of Theorem 4. Our proof follows that of Theorem 1 in [23]. For a square matrix A , let A^- be the matrix with zeros on the diagonal and off-diagonal elements equal to those of A . Also, set $\|A\|_1 = \sum_{j,k} |A_{jk}|$. Let $\hat{\Xi}$ be the $pL \times pL$ block diagonal matrix with the estimates $\hat{\Xi}_l$ along the diagonal, and set $Q_l(\Upsilon_l) = \text{trace}(\hat{R}_l \Upsilon_l) - \log(|\Upsilon_l|) + \gamma \|\Upsilon_l^-\|_1$. Then

$$\hat{\Xi} = \arg \min_{\substack{\Upsilon = \text{diag}(\Upsilon_1, \dots, \Upsilon_L) \\ \Upsilon_l = \Upsilon_l^\top, \Upsilon_l \succ 0}} Q(\Upsilon), \quad Q(\Upsilon) = \sum_{l=1}^L Q_l(\Upsilon_l).$$

Now, set $\hat{\Delta}_l = \hat{\Xi}_l - \Xi_l$ and $\hat{\Delta} = \text{diag}(\hat{\Delta}_1, \dots, \hat{\Delta}_L)$. Then $\hat{\Delta}$ uniquely minimizes $W(\Delta) = Q(\Delta + \Xi) - Q(\Xi)$ among all block diagonal, symmetric positive definite Δ . Furthermore, $W(0) = 0 \geq W(\hat{\Delta})$. Now, let $r_n^2 = (d_L^2 q_L)/(n\pi_L^2)$ and define

$$\Theta_n(R) = \left\{ \Delta = \text{diag}(\Delta_1, \dots, \Delta_L) : \Delta_l = \Delta_l^\top, \Delta_l \succ 0, \|\Delta\|_F^2 = Rr_n^2 \right\}.$$

The idea is to show that, for any $\epsilon > 0$, there exists large enough R such that

$$P\left(\inf_{\Delta \in \Theta_n(R)} W(\Delta) > 0\right) \geq 1 - \epsilon,$$

which will prove the result.

Let $\tilde{\Delta}_l$ be the vectorized version of Δ_l , and set

$$g_l(\Delta_l) = \tilde{\Delta}_l^\top \left[\int_0^1 (1-v)(\Xi_l + v\Delta_l)^{-1} \otimes (\Xi_l + v\Delta_l) dv \right] \tilde{\Delta}_l,$$

\otimes denoting the Kronecker product. Let $S_l = \{(j, k) : (\Xi_l)_{jk} \neq 0, j \neq k\}$ and write Δ_{l, S_l} for the submatrix corresponding to elements $(j, k) \in S_l$, and similarly for Δ_{l, S_l^c} . Let $b > 0$ be a lower bound for all eigenvalues of the correlation matrices R_l guaranteed by assumption (A2). Following arguments of [23], we have

$$W(\Delta) = \sum_{l=1}^L \left\{ \text{trace}(\Delta_l(\hat{R}_l - R_l)) + g_l(\Delta_l) + \gamma[\|(\Xi_l + \Delta_l)^-\|_1 - \|\Xi_l^-\|_1] \right\},$$

along with the inequalities

$$\begin{aligned} \left| \sum_{l=1}^L \text{trace}(\Delta_l(\hat{R}_l - R_l)) \right| &\leq \left(\sum_{l=1}^L \|\Delta_l^-\|_1 \right) \max_{l=1, \dots, L} \max_{j \neq k} |\hat{r}_{ljk} - r_{ljk}|, \\ g_l(\Delta_l) &\geq \frac{b^2}{4} \|\Delta_l\|_F^2, \\ \gamma[\|(\Xi_l + \Delta_l)^-\|_1 - \|\Xi_l^-\|_1] &\geq \gamma[\|\Delta_{l, S_l}^-\|_1 - \|\Delta_{l, S_l^c}^-\|_1]. \end{aligned}$$

Next, by Corollary 2, there exists $C > 0$ such that

$$P \left(\max_{l=1, \dots, L} \max_{j \neq k} |\hat{r}_{ljk} - r_{ljk}| \leq C \frac{r_n}{q_L^{1/2}} \right) \geq 1 - \epsilon.$$

For some $\eta < 1$, set $\gamma = (Cr_n)/(q_L^{1/2}\eta)$. Then, with probability at least $1 - \epsilon$, for $\Delta \in \Theta_n(R)$,

$$\begin{aligned} W(\Delta) &\geq \frac{b^2}{4} \|\Delta\|_F^2 - Cr_n q_L^{-1/2} \|\Delta^-\|_1 + \gamma[\|\Delta_{l, S_l}^-\|_1 - \|\Delta_{l, S_l^c}^-\|_1] \\ &= \frac{b^2}{4} \|\Delta\|_F^2 - Cr_n q_L^{-1/2} [1 - \eta^{-1}] \sum_{l=1}^L \|\Delta_{l, S_l}^-\|_1 - Cr_n q_L^{-1/2} [1 + \eta^{-1}] \sum_{l=1}^L \|\Delta_{l, S_l}^-\|_1. \end{aligned}$$

The second term above is positive, so it can be removed from the lower bound. Next, by Cauchy-Schwarz

$$\sum_{l=1}^L \|\Delta_{l, S_l}^-\|_1 \leq \sum_{l=1}^L \sqrt{2|E_l|} \|\Delta_{l, S_l}^-\|_F \leq \sqrt{2q_L} \|\Delta^-\|_F.$$

Thus, we have shown that with probability at least $1 - \epsilon$, for any $\Delta \in \Theta_n(R)$,

$$\begin{aligned} W(\Delta) &\geq \frac{b^2}{4} \|\Delta\|_F^2 - \sqrt{2} C r_n (1 + \eta^{-1}) \|\Delta^-\|_F \\ &\geq \|\Delta\|_F^2 \left(\frac{b^2}{4} - \frac{\sqrt{2} C r_n (1 + \eta^{-1})}{\sqrt{R} r_n} \right) \\ &= \|\Delta\|_F^2 \left(\frac{b^2}{4} - \sqrt{\frac{2}{R}} C (1 + \eta^{-1}) \right), \end{aligned}$$

which will be positive for large enough R . This concludes the proof. \square

Algorithm for Section 6

Algorithm 1: Pseudocode to create the edge sets E_1, \dots, E_M

Input : Graph $G = (V, E)$ with nodes $V = \{1, \dots, p\}$ and edge set E

Input : Number of basis M

Input : Proportion of common edges τ

Output: E_1, \dots, E_M

1 Set $E_c \leftarrow$ random subset of size $\tau|E|$ from E

2 Set $E_l \leftarrow E_c$ for $l = 1, \dots, M$

3 Set $l \leftarrow 1, B \leftarrow 1$

4 **for** $e \in E \setminus E_c$ **do**

5 $E_l \leftarrow E_l \cup e$

6 $l \leftarrow l + 1$

7 **if** $l > B$ **then**

8 $l \leftarrow 1$

9 $B \leftarrow (B + 1) \bmod M$

10 **end**

11 Return E_1, \dots, E_M

Results for Very Sparse Graphs for Section 6

This section includes results with a power law distribution parameter $\pi = 0.025$ and a proportion of common edges $\tau = 0$.

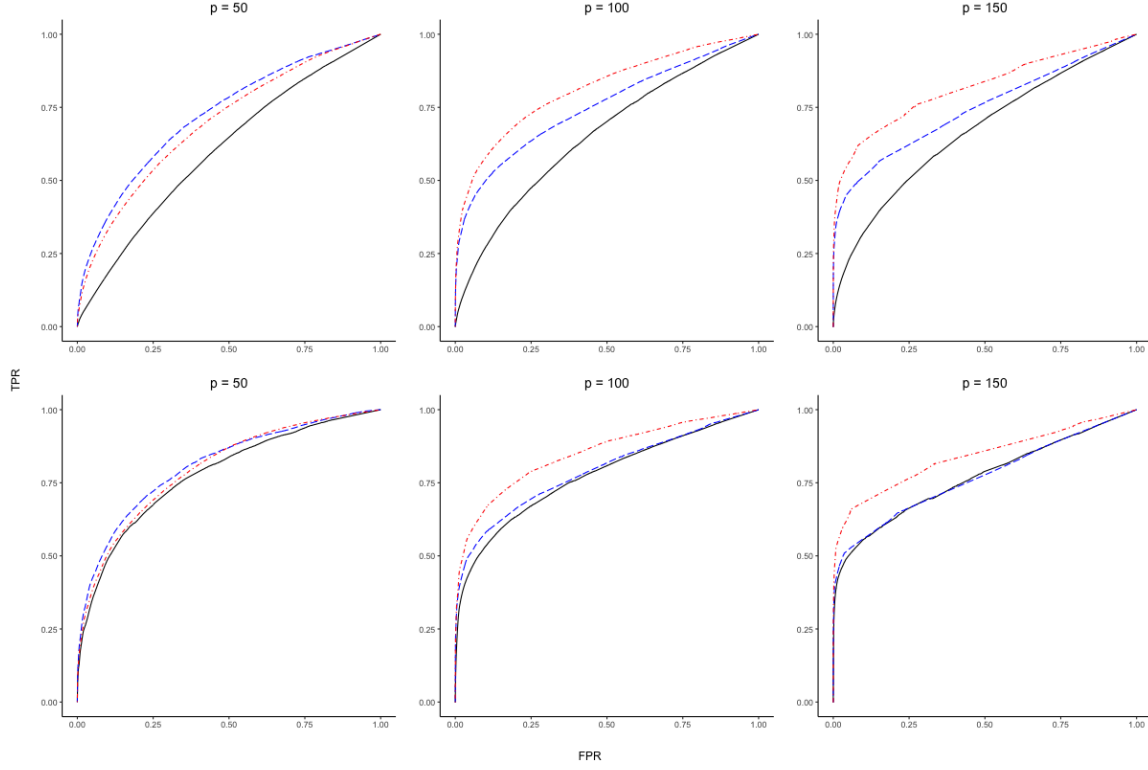


Figure 4: *Expected ROC curves for psFGGM and FGGM under Σ_{ps} (top) and Σ_{non-ps} (bottom) for $p = 50, 100, 150$ and $n = p/2$. We see psFGGM (---) and FGGM (—) at 90% of variance and psFGGM (-.-) at 95% of variance explained.*

Table 3: Mean AUC (standard error) values for Figure 4

Σ	p	AUC			AUC15 [†]		
		FGGM _{90%}	psFGGM _{90%}	psFGGM _{95%}	FGGM _{90%}	psFGGM _{90%}	psFGGM _{95%}
Σ_{ps}	50	0.61(0.06)	0.73(0.05)	0.70(0.05)	0.15(0.06)	0.31(0.08)	0.27(0.07)
Σ_{ps}	100	0.65(0.02)	0.75(0.03)	0.81(0.02)	0.21(0.03)	0.44(0.03)	0.50(0.04)
Σ_{ps}	150	0.67(0.02)	0.74(0.02)	0.82(0.02)	0.26(0.02)	0.47(0.03)	0.57(0.03)
$\Sigma_{\text{non-ps}}$	50	0.78(0.05)	0.81(0.05)	0.80(0.05)	0.40(0.07)	0.46(0.08)	0.42(0.08)
$\Sigma_{\text{non-ps}}$	100	0.77(0.02)	0.79(0.02)	0.85(0.03)	0.47(0.03)	0.52(0.04)	0.59(0.05)
$\Sigma_{\text{non-ps}}$	150	0.77(0.02)	0.77(0.02)	0.84(0.02)	0.51(0.03)	0.52(0.03)	0.63(0.04)

[†]AUC15 is AUC computed for FPR in the interval $[0, 0.15]$, normalized to have maximum area 1.

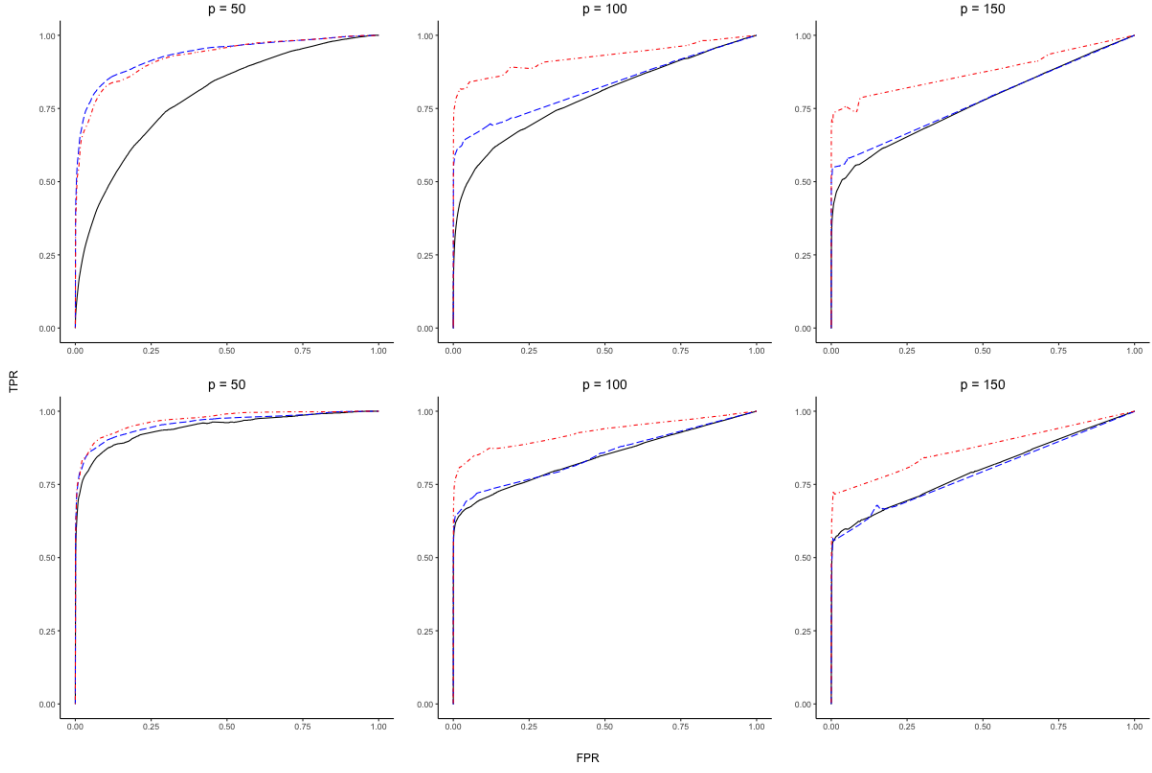


Figure 5: Expected ROC curves for $psFGGM$ and $FGGM$ under Σ_{ps} (top) and Σ_{non-ps} (bottom) for $p = 50, 100, 150$ and $n = 1.5p$. We see $psFGGM$ (---) and $FGGM$ (—) at 90% of variance and $psFGGM$ (-.-) at 95% of variance explained.

Table 4: Mean AUC (standard error) values for Figure 5

Σ	p	AUC			AUC15 [†]		
		FGGM _{90%}	psFGGM _{90%}	psFGGM _{95%}	FGGM _{90%}	psFGGM _{90%}	psFGGM _{95%}
Σ_{ps}	50	0.79(0.05)	0.93(0.03)	0.92(0.03)	0.39(0.08)	0.78(0.06)	0.74(0.07)
Σ_{ps}	100	0.79(0.02)	0.82(0.02)	0.92(0.02)	0.52(0.03)	0.65(0.03)	0.83(0.03)
Σ_{ps}	150	0.77(0.02)	0.78(0.02)	0.87(0.02)	0.53(0.02)	0.58(0.02)	0.75(0.03)
$\Sigma_{\text{non-ps}}$	50	0.94(0.03)	0.96(0.02)	0.96(0.02)	0.82(0.05)	0.86(0.06)	0.86(0.05)
$\Sigma_{\text{non-ps}}$	100	0.84(0.02)	0.85(0.02)	0.93(0.02)	0.68(0.03)	0.69(0.04)	0.83(0.03)
$\Sigma_{\text{non-ps}}$	150	0.79(0.02)	0.80(0.02)	0.87(0.02)	0.60(0.03)	0.60(0.04)	0.74(0.03)

[†]AUC15 is AUC computed for FPR in the interval $[0, 0.15]$, normalized to have maximum area 1.

References

- [1] John AD Aston, Davide Pigoli, Shahin Tavakoli, et al. Tests for separability in non-parametric covariance operators of random surfaces. *The Annals of Statistics*, 45(4): 1431–1461, 2017.
- [2] Deanna M. Barch, Gregory C. Burgess, Michael P. Harms, Steven E. Petersen, Bradley L. Schlaggar, Maurizio Corbetta, Matthew F. Glasser, Sandra Curtiss, Sachin Dixit, Cindy Feldt, Dan Nolan, Edward Bryant, Tucker Hartley, Owen Footer, James M. Bjork, Russ Poldrack, Steve Smith, Heidi Johansen-Berg, Abraham Z. Snyder, and David C. Van Essen. Function in the human connectome: Task-fMRI and individual differences in behavior. *NeuroImage*, 80:169 – 189, 2013.
- [3] Denis Bosq. *Linear Processes in Function Spaces: Theory and Applications*. Springer-Verlag, New York, 2000.

- [4] Kehui Chen, Pedro Delicado, and Hans-Georg Müller. Modeling function-valued stochastic processes, with applications to fertility dynamics. Journal of the Royal Statistical Society, Series B (Theory and Methodology), 79:177–196, 2017.
- [5] Jeng-Min Chiou and Hans-Georg Muller. Linear manifold modelling of multivariate functional data. Journal of the Royal Statistical Society: Series B (Statistical Methodology), 76:605–626, 2014.
- [6] Jeng-Min Chiou, Yu-Ting Chen, and Ya-Fang Yang. Multivariate functional principal component analysis: A normalization approach. Statistica Sinica, pages 1571–1596, 2014.
- [7] Jeng-Min Chiou, Ya-Fang Yang, and Yu-Ting Chen. Multivariate functional linear regression and prediction. Journal of Multivariate Analysis, 146:301–312, 2016.
- [8] Patrick Danaher, Pei Wang, and Daniela M Witten. The joint graphical lasso for inverse covariance estimation across multiple classes. Journal of the Royal Statistical Society: Series B (Statistical Methodology), 76(2):373–397, 2014.
- [9] Joel A. Dubin and Hans-Georg Müller. Dynamical correlation for multivariate longitudinal data. Journal of the American Statistical Association, 100(471):872–881, 2005.
- [10] J. H. Friedman. A variable span scatterplot smoother. Technical Report 5, Stanford University, 1984.
- [11] Matthew F. Glasser, Stamatios N. Sotiropoulos, J. Anthony Wilson, Timothy S. Coalson, Bruce Fischl, Jesper L. Andersson, Junqian Xu, Saad Jbabdi, Matthew Webster, Jonathan R. Polimeni, David C. Van Essen, and Mark Jenkinson. The minimal pre-processing pipelines for the human connectome project. NeuroImage, 80:105–124,

2013. ISSN 1053-8119. URL <http://www.sciencedirect.com/science/article/pii/S1053811913005053>.

- [12] Matthew F. Glasser, Timothy S. Coalson, Emma C. Robinson, Carl D. Hacker, John Harwell, Essa Yacoub, Kamil Ugurbil, Jesper Andersson, Christian F. Beckmann, Mark Jenkinson, Stephen M. Smith, and David C. Van Essen. A multi-modal parcellation of human cerebral cortex. Nature, 536:171–178, 2016.
- [13] Clara Happ and Sonja Greven. Multivariate functional principal component analysis for data observed on different (dimensional) domains. Journal of the American Statistical Association, 113(522):649–659, 2018.
- [14] Tailen Hsing and Randall Eubank. Theoretical Foundations of Functional Data Analysis, with an Introduction to Linear Operators. John Wiley & Sons, 2015.
- [15] Mladen Kolar and Eric Xing. On time varying undirected graphs. In Proceedings of the Fourteenth International Conference on Artificial Intelligence and Statistics, pages 407–415, 2011.
- [16] Bing Li and Eftychia Solea. A nonparametric graphical model for functional data with application to brain networks based on fmri. Journal of the American Statistical Association, pages 1–19, 2018.
- [17] Brian Lynch and Kehui Chen. A test of weak separability for multi-way functional data, with application to brain connectivity studies. Biometrika, 105(4):815–831, 2018.
- [18] Jie Peng, Pei Wang, Nengfeng Zhou, and Ji Zhu. Partial correlation estimation by joint sparse regression models. Journal of the American Statistical Association, 104(486):735–746, 2009.

- [19] Alexander Petersen and Hans-Georg Müller. Fréchet integration and adaptive metric selection for interpretable covariances of multivariate functional data. Biometrika, 103: 103–120, 2016.
- [20] Xinghao Qiao, Cheng Qian, Gareth M James, and Shaojun Guo. Doubly functional graphical models in high dimensions. Preprint, 2018.
- [21] Xinghao Qiao, Shaojun Guo, and Gareth M James. Functional graphical models. Journal of the American Statistical Association, 114(525):211–222, 2019.
- [22] Huitong Qiu, Fang Han, Han Liu, and Brian Caffo. Joint estimation of multiple graphical models from high dimensional time series. Journal of the Royal Statistical Society: Series B (Statistical Methodology), 78(2):487–504, 2016.
- [23] Adam J Rothman, Peter J Bickel, Elizaveta Levina, Ji Zhu, et al. Sparse permutation invariant covariance estimation. Electronic Journal of Statistics, 2:494–515, 2008.
- [24] Jane-Ling Wang, Jeng-Min Chiou, and Hans-Georg Müller. Functional data analysis. Annual Review of Statistics and its Application, 3:257–295, 2016.
- [25] W. Yang, H.-G. Müller, and U. Stadtmüller. Functional singular component analysis. Journal of the Royal Statistical Society: Series B (Statistical Methodology), 73:303–324, 2011.
- [26] Fang Yao, Hans-Georg Müller, and Jane-Ling Wang. Functional data analysis for sparse longitudinal data. Journal of the American Statistical Association, 100(470): 577–590, 2005. ISSN 0162-1459.
- [27] Xiaoke Zhang and Jane-Ling Wang. From sparse to dense functional data and beyond. The Annals of Statistics, 44:2281–2321, 2016.

- [28] Shuheng Zhou, John Lafferty, and Larry Wasserman. Time varying undirected graphs. Machine Learning, 80(2-3):295–319, 2010.
- [29] Hongxiao Zhu, Nate Strawn, and David B. Dunson. Bayesian graphical models for multivariate functional data. Journal of Machine Learning Research, 17(204):1–27, 2016.